ACS Catalysis

pubs.acs.org/acscatalysis Research Article

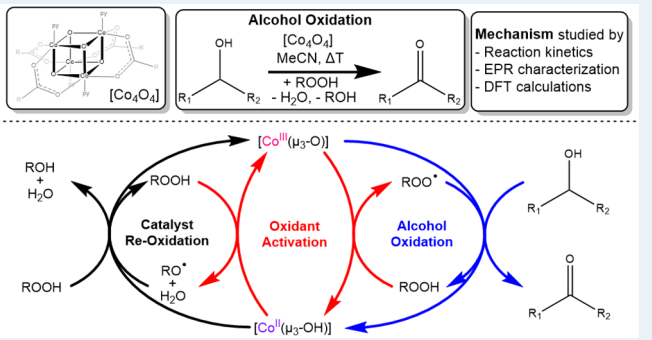
Comparative Study on the Catalytic Activity of Molecular $[Co_4^{III}O_4]$ Heterocubanes in Alcohol Oxidation Reactions in Solution

Timo Fockenberg,[#] Niklas Sülzner,[#] Takuma Sato, Dongsheng Zhang, Akhil Hareendran, Jill M. Reher, Joana Tewes, Alexander Schnegg,* Martin Muhler, Christof Hättig,* and Stephan Schulz*

Cite This: *ACS Catal.* 2026, 16, 6355−6367 Read Online

ACCESS | Metrics & More | Article Recommendations | Supporting Information

ABSTRACT: A comparative study on the catalytic oxidation of 2-propanol (*i*-PrOH), benzyl alcohol (BnOH), and cinnamyl alcohol (CnOH) in solution under moderate reaction conditions (65−150 °C) using two tetranuclear Co^{III}-oxo complexes $[Co_4O_4(O_2CR)_4(py)_4]$ (R = Me **1**, Et **2**, py = pyridine) and three different oxidants (O_2, H_2O_2, *tert*-butyl hydroperoxide (TBHP)) is reported. TBHP is the most active oxidant, resulting in turnover frequency (TOF) values ranging from 40 to 100 h^{-1}. The slightly larger carboxylate ligand in complex **2** favors aldehyde selectivity but slightly decreases the conversion rates as was confirmed by GC analyses. Mechanistic investigations (*in situ* ^1H NMR, EPR) confirm the active participation of transiently formed radicals in these reactions. Using quantum-chemical calculations, a detailed mechanistic understanding of the catalytic reactions was gained that fully agrees with the experimental observations. Two interrelated catalytic cycles were identified: one for the oxidant activation and one for the alcohol oxidation. Catalytic TBHP oxidation reactions are initiated via Haber-Weiss activation of TBHP, resulting in the formation of *tert*-butyl peroxyl radicals (*t*-BuOO•), and simultaneous reduction of Co^{III} to Co^{II}.



KEYWORDS: *cobalt(III) complexes, catalysis, alcohol oxidation, mechanism, DFT calculations*

Downloaded via RUHR UNIVERSITAET BOCHUM on April 24, 2026 at 07:42:18 (UTC).
See https://pubs.acs.org/sharingguidelines for options on how to legitimately share published articles.

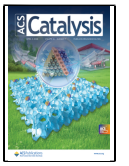
INTRODUCTION

Spinel-type cobalt oxide nanoparticles belong to the most efficient earth-abundant catalysts for water oxidation (water splitting)[1] and the aerobic oxidation of organic substrates[2,3] such as epoxidation of olefins and alcohol oxidation. Co_3O_4-catalyzed alcohol oxidation reactions typically showed the highest activities for benzyl alcohol (BnOH) oxidation, particularly for large Co_3O_4 particles with low Co^{III} to Co^{II} ratios and a large number of oxygen vacancies.[4] Co^{III} is the active species in BnOH oxidation,[5] hence the conversion of Co^{II} into Co^{III} represents the (often rate-determining) activation step. Moreover, the catalytic activity in 2-propanol oxidation was strongly affected by the surface structure (crystal facet) of the spinel nanoparticles.[6]

Tetranuclear cobalt-oxo complexes with a central $[Co_4^{III}O_4]$ heterocubane-type core, in which four Co^{III} atoms are bridged by four oxygen atoms (μ_3-O), have often been studied as molecular model catalysts in oxidation reactions.[7] They mimic not only structurally the active site of the oxygen-evolving photosystem II, which is a molecular Mn_4CaO_5 cluster complex,[8] but also bear a structural resemblance to a subunit of cobalt oxide CoO_x and are therefore considered as molecular model systems for heterogeneous cobalt oxide nanoparticles. The same is true for structurally related tetranuclear $[Co_4^{II}O_4]$ complexes containing four Co^{II} centers.[9]

Molecular $[Co_4O_4]$ complexes show several advantages compared to cobalt oxides, which render them very interesting for mechanistic studies:[7,10−14] (i) the Co centers in these stable multimetallic complexes can easily be oxidized to higher oxidation states (*e.g.*, Co^{IV}, Co^{V}) under catalytic conditions,[7] which is a prerequisite for multielectron and multiproton transfer reactions; (ii) the stabilizing organic ligands of such complexes can easily be varied, allowing for a fine-tuning of the physicochemical, and hence catalytic, properties of such complexes; and finally (iii) molecular complexes offer more (spectroscopic) options to gain mechanistic insights compared to heterogeneous spinel-type catalysts due to their solubility in organic solvents. However, overcoming the oxidative instability of many ligands at high anodic potentials is still challenging,

Received: November 12, 2025
Revised: February 17, 2026
Accepted: March 6, 2026
Published: March 15, 2026



ACS Publications © 2026 American Chemical Society

https://doi.org/10.1021/acscatal.5c07998
ACS Catal. 2026, 16, 6355−6367

although, Patzke et al. recently introduced concepts for their immobilization into conductive polymer matrices.[15]

$[Co_4^{III}O_4]$ complexes are promising catalysts in water oxidation reactions.[15,16] Mechanistic studies revealed that $[Co_3^{III}Co^{IV}O_4(OAc)_4(py)_4]^+$ ($\mathbf{1}^+$) serves as a model for the paramagnetic intermediate formed during water oxidation.[7,17] $\mathbf{1}^+$ is reduced to $[Co_4^{III}O_4(OAc)_4(py)_4]$ **1** by stoichiometric reaction with hydroxide anions, concomitant with the evolution of molecular oxygen,[18] indicating that the Co^{IV} center in $\mathbf{1}^+$ is responsible for O−O bond formation. However, further studies also showed that $\mathbf{1}^+$ most likely disproportionates to a doubly oxidized state, formally $[Co_2^{III}Co_2^{IV}]$ or $[Co_3^{III}Co^{V}]$, before oxygen (O_2)evolution.[7,18,19] A detailed reaction mechanism was proposed,[7,20,21] with the Co^{IV} species **1**(OOH) as the most likely intermediate in the catalytic cycle. $[Co_4^{III}O_4]$ complexes were also applied in the oxidation of *α*-pinene,[22] benzyl alcohol derivates, ethylbenzene and *p*-xylene, styrene, and diphenylmethane,[10,22−26] but the reaction mechanisms are yet unknown.

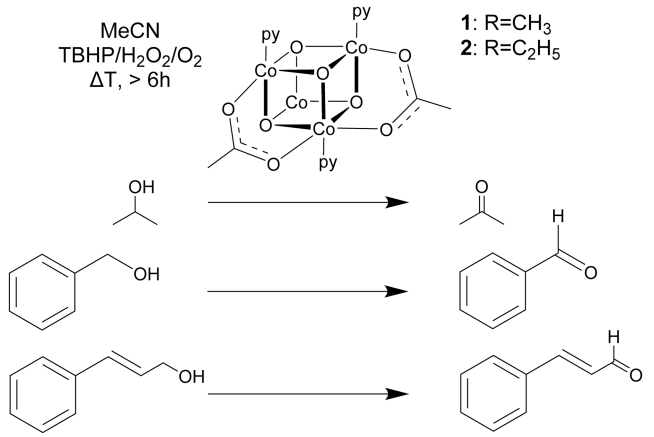
We are interested in developing a mechanistic understanding of alcohol oxidation reactions in solution using molecular cobalt-oxo complexes and herein report the results of a comparative study, in which catalytic oxidation reactions of 2-propanol (*i*-PrOH), benzyl alcohol (BnOH) and cinnamyl alcohol (CnOH) in acetonitrile (MeCN) solution with three different oxidants (O_2, H_2O_2, TBHP) and catalytic amounts of two tetranuclear complexes $[Co_4O_4(O_2CR)_4(py)_4]$ (R = Me **1** and Et **2**) were investigated.[13] A combination of *in situ* fourier transform infrared (FT-IR) and *in situ* ^{1}H nuclear magnetic resonance (NMR) spectroscopy experiments, GC analyses as well as electron paramagnetic resonance (EPR) studies accompanied by density functional theory (DFT) calculations was used to elucidate the catalytic reactions and to gain a mechanistic understanding.

RESULTS AND DISCUSSION

Catalytic Studies

Complexes **1** or **2** (0.1 mol %) and the respective alcohol were dissolved in dry and oxygen-free MeCN under an argon atmosphere. Equimolar amounts of H_2O_2 (30% in H_2O) or TBHP were added, and the resulting solution was heated to 82 °C within 15 min and stirred for 6 h (Scheme 1). Oxidation reactions with O_2 were performed under 10 bar O_2 pressure in a closed Parr autoclave at 150 °C. All reactions were monitored by *in situ* FT-IR spectroscopy, which was used as qualitative screening method to identify oxidation reaction products including the possible formation of CO_2 resulting from complete oxidation.

Scheme 1. Schematic Representation of the Catalytic Reactions



H_2O_2 completely failed in the alcohol oxidation reactions, even with varying catalyst concentrations of complex **1** (0.1 mol %, 1 mol %) and H_2O_2/alcohol molar ratios (1:1, 2:1), respectively. Only thermally induced decomposition of H_2O_2 into H_2O and O_2 was observed starting at 46 °C, indicated by an increase of the H−O−H scissors bending of water (1636.6 cm^{-1})[27] and a decrease of O−H bending[28] mode of H_2O_2 (1364.8 cm^{-1}), respectively (Figure S6).

O_2 failed to oxidize *i*-PrOH even under high O_2 pressure (20 bar) and high reaction temperatures up to 180 °C (temperature limited by thermal stability of the complex **1**), whereas BnOH and CnOH were oxidized at 150 °C and an O_2 pressure of 10 bar. This was proven by a steady O_2 uptake (loss of O_2 pressure in the autoclave) and a steady growth of the carbonyl absorption band (benzaldehyde 1704 cm^{-1}; cinnamaldehyde 1680 cm^{-1}) in the FT-IR spectra (Figures S3−S5).

In remarkable contrast, all three alcohols were oxidized by complex **1** with TBHP as oxidant as was confirmed by the appearance of a distinctive carbonyl absorption band of the corresponding aldehyde (acetone 1712 cm^{-1}; benzaldehyde 1704 cm^{-1}; cinnamaldehyde 1680 cm^{-1}; Figures 1a, S1, S2) in the *in situ* FT-IR spectra. Control experiments proved that complexes **1** and **2** are stable toward decomposition in MeCN solutions, and both complexes only catalyze the alcohol oxidation in the presence of TBHP, while TBHP only catalyzes alcohol oxidation in the presence of complexes **1** or **2**. We did not notice full oxidation of any alcohol to CO_2 in the experiments. We furthermore investigated the stability of complexes **1** and **2** toward TBHP and observed the formation of Co_3O_4 particles according to PXRD studies (Figure S17) after heating the complexes with 50 equiv of TBHP up to 82 °C for 10 h.

Since TBHP turned out to be the most active oxidant in all alcohol oxidation reactions, conversion, aldehyde yields, selectivities and TOF values of these reactions were semi-quantitatively determined by *in situ* ^{1}H NMR spectroscopy via integration of the characteristic resonances of the resulting aldehyde (Table 1).

The progress of 2-propanol oxidation was monitored by the decreasing intensity of the Me resonance of the alcohol (1.16 ppm) and the increasing Me resonance of acetone (2.14 ppm, Figure 1). The conversion to acetone after 6.5 h and the TOF were higher with complex **1** (46.9%, TOF = 63.4) than with complex **2** (35.3%, TOF = 47.7), but the acetone selectivity was 100% for both complexes.

The oxidation of CnOH was analyzed by monitoring the methylene proton signal of alcohol (4.22 ppm) and the corresponding aldehyde (9.68 ppm). The conversion to cinnamaldehyde was incomplete after 6.5 h (conversion 76.3% **1**; 49.9% **2**), and the formation of multiple side products proved the low selectivity of this oxidation reaction, most likely resulting from further oxidation of the conjugated alkene moiety. These findings agree with previously reported product patterns (cinnamaldehyde, 3-phenylglycidol, cinnamaldehyde epoxide, benzaldehyde) observed for cinnamyl alcohol oxidation with Co_3O_4,[29] although individual species could not be unambiguously assigned based on ^{1}H NMR spectroscopy.

https://doi.org/10.1021/acscatal.5c07998
ACS Catal. 2026, 16, 6355−6367

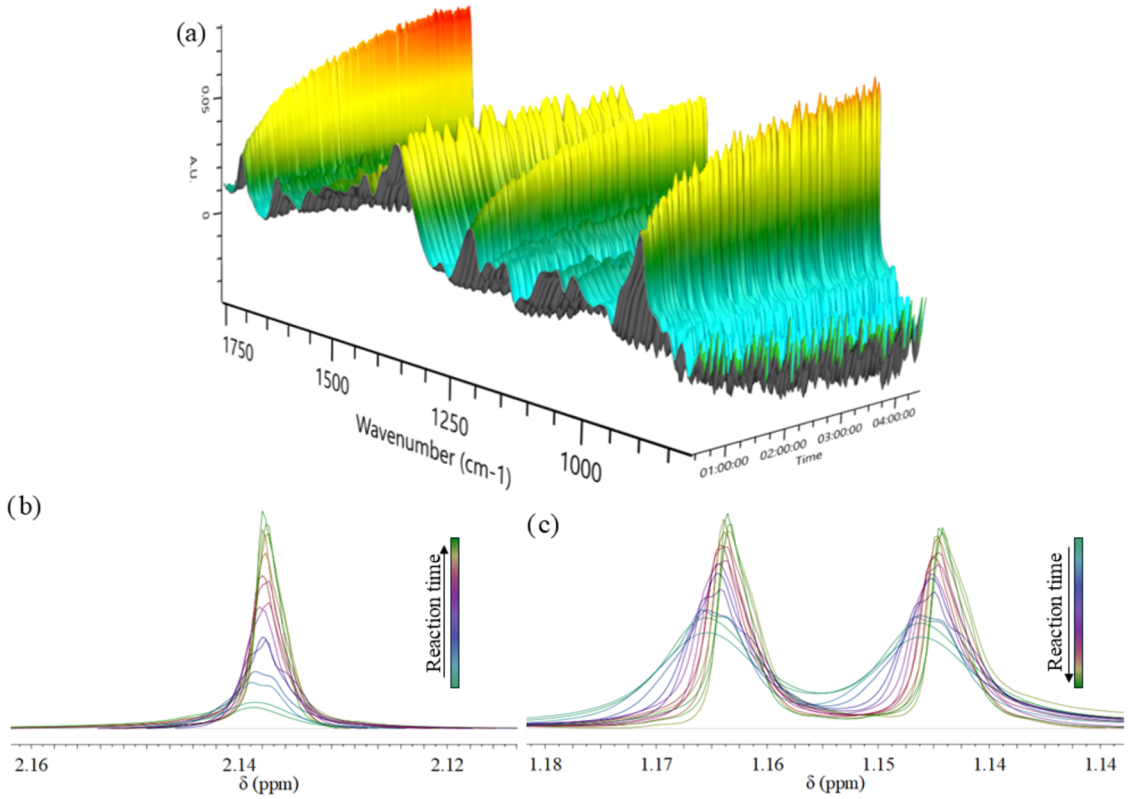


Figure 1. (a) *In situ* reaction monitoring (800 cm^{-1} − 1800 cm^{-1}) of *i*-PrOH oxidation with TBHP (1:1) and 0.1 mol % of complex **1**. Increasing signals: 1712, 1364, 1204, 908 cm^{-1}; decreasing signals: 1279, 1095, 948, 844 cm^{-1}. *In situ* ^{1}H NMR spectra recorded every 30 min show the (b) increasing Me resonance of acetone at 2.14 ppm and (c) decreasing Me resonance of *i*-PrOH at 1.16 ppm.

Table 1. Conversion (*X*), Aldehyde Yield (*Y*), and Selectivity (*S*) and TOF of Catalytic Alcohol Oxidation Reactions Using TBHP and Complexes 1 and 2 under Argon Atmosphere at 65 °C for 6.5 h (Molar Ratio TBHP/Alcohol 1:1)

complex	alcohol	*X* [%]	*Y* [%]	*S* [%]	TOF [h^{-1}]
1	2-propanol	46.9	46.9	100	63.4
	benzyl alcohol	47.2	25.2	53.3	63.8
	cinnamyl alcohol	76.3	10.8	14.2	103.2
2	2-propanol	35.3	35.3	100	47.7
	benzyl alcohol	31.9	24.7	77.4	43.1
	cinnamyl alcohol	49.9	18.1	36.2	67.4

The oxidation of BnOH with complexes **1** and **2** showed a lower aldehyde selectivity compared to *i*-PrOH and a higher selectivity compared to CnOH; however, the TOF values were the lowest. Integration of the benzylic CH_2 resonance (4.65 ppm) and the benzaldehyde C(H)O resonance (10.05 ppm) indicated incomplete conversions after 6.5 h (conversion of 47.2% **1**; 31.9% **2**). Additional signals, notably an aromatic resonance at 8.16 ppm, prove the formation of benzoic acid due to overoxidation of benzaldehyde.

The quantitative analysis of the reactions with complexes **1** and **2** were further supported by gas chromatography (GC) measurements addressing the carbon balances (Table S1, Figure S16). The oxidation of *i*-PrOH using complex **1** resulted in a relatively higher acetone yield (0.37 mol·L^{-1}) compared with complex **2** in agreement with the *in situ* ^{1}H NMR measurements. Reactions with both complexes yielded acetone as the main product with a relatively closed carbon balance (>90%). As shown by *in situ* ^{1}H NMR spectroscopy studies, both complexes also formed lower amounts of cinnamaldehyde (complex **1**: 0.247 mol·L^{-1}; complex **2**: 0.233 mol·L^{-1}) during CnOH oxidation determined by GC analyses. However, the yields determined by GC are higher than those determined by *in situ* ^{1}H NMR, which can be explained by the higher detection sensitivity. Minor amounts of benzaldehyde as a side product resulting from C−C bond cleavage reaction were also identified and quantified by GC, further supporting the ^{1}H NMR observations, where incomplete conversion to cinnamaldehyde (lower carbon balance <61%) and side product formation (mainly benzaldehyde) were observed after 6.5 h. Similar trends were observed in BnOH oxidation, where low benzaldehyde amounts were detected (complex **1**: 0.198 mol·L^{-1}; complex **2**: 0.227 mol·L^{-1}). Despite the additional signals observed by *in situ* ^{1}H NMR spectroscopy, which were addressed to the formation of benzoic acid, its formation was not identified by GC measurements. This may be explained due to the tendency of benzoic acid to undergo ligand exchange reactions and subsequently bind as a chelating ligand with the complexes, which are then inseparable and not detected by GC anymore. The ligand exchange reactions were proven by *in situ* ^{1}H NMR spectroscopy in a control experiment of complex **1** with benzoic acid. In agreement with the *in situ* ^{1}H NMR measurements, the relatively lower carbon balance (<61%) in BnOH oxidation points to benzoic acid as the side product. In conclusion, the GC measurements support the relative product distributions observed by the *in situ* ^{1}H NMR measurements and confirm that carbon balances are not fully closed for BnOH and CnOH oxidation.

https://doi.org/10.1021/acscatal.5c07998
ACS Catal. 2026, 16, 6355−6367

Additional control experiments were conducted and monitored by *in situ* FT-IR spectroscopy (carbonyl formation at 1703 cm^{-1}) to investigate the potential decomposition of complex **1** during the oxidation reactions, which might explain the low TOF values. Addition of a second portion of either complex **1** (Figure S9) or TBHP (Figure S7) after 1 h, after which the initial carbonyl formation rate had reached a constant level, had no effect on the carbonyl formation, whereas the addition of a second portion of BnOH resulted in a continued increase of the carbonyl signal (Figure S8). These observations suggest that the deceleration of the reaction can be primarily attributed to the reduced substrate accessibility rather than the catalyst deactivation, even though the catalytically active species is not necessarily identical with the cubane-type complexes **1** or **2** but probably structurally closely related as previously suggested.[30] Unfortunately, despite several attempts we did not succeed in the isolation of complexes **1** or **2** after the catalytic reaction with 10 equiv of TBHP and the respective alcohol from the resulting solution, most likely due to the small amounts of both complexes used in these reactions. Moreover, the strong accumulation of benzoic acid and the continual generation of water in the oxidation of BnOH are plausible contributors to catalyst inhibition and rate deceleration in these TBHP systems. Both complexes **1** and **2** were found to slowly react with benzoic acid with formation of benzoate-substituted compounds, whose molecular structure could not be clarified yet. Even though these ligand substitution reactions are slower than the catalytic reactions, partial cluster fragmentation or the build-up of inhibitory species cannot be fully excluded.

Several trends were found when the catalytic activity of complexes **1** and **2**. Complex **1** showed higher conversions and higher TOF values for the oxidation of a given alcohol than complex **2**, whereas the opposite trend was observed for the aldehyde selectivity, which was typically higher with complex **2** than with complex **1**. The gain in selectivity from complex **1** to complex **2** most likely results from the small increase in ligand size as was reported previously.[31,32] In addition, the yield and TOF values of *i*-PrOH and BnOH oxidation reactions were almost the same for both complexes **1** and **2**, whereas CnOH was found to be more easily oxidized by both complexes, as expressed by higher conversion and TOF values, respectively. Unfortunately, the aldehyde selectivity in CnOH oxidation was even lower than for BnOH oxidation. Our study clearly proves that *i*-PrOH is more difficult to oxidize[3,33] compared to the aryl alcohols, but the latter can undergo further oxidation to the acids or other products.[29]

Das et al. previously studied BnOH oxidation using sterically more demanding benzoate-substituted (and pyridine derivatives) tetranuclear $[Co_4^{III}O_4]$ complexes and TBHP.[30] High aldehyde selectivity (90%) and high TOF values (up to 110 h^{-1}) were obtained after 5 h at a reaction temperature of 82 °C. With respect to our results obtained with complexes **1** and **2** and TBHP in the BnOH oxidation, the higher selectivity most likely resulted from the higher steric demand of the complexes,[31] while the higher activities could result from the higher catalyst concentration and the higher TBHP/BnOH ratio (3:1). Chakrabarty et al. assumed that both substrate conversion and product yield depend on the amount of TBHP used in the reaction.[30]

To ensure comparability between both studies, we closely reproduced the catalytic procedure reported by Das et al. and studied the BnOH oxidation with three equivalents of TBHP and 0.2 mol % of complex **1**. However, since we monitored the reaction by *in situ* ^{1}H NMR spectroscopy, the reaction temperature was limited to 75 °C (instead of 82 °C). Moreover, we observed a notably decreasing reaction rate after 2 h, and therefore, the reaction was terminated after 2.5 h. Das et al. reported aldehyde yields of up to 70% after 2.5 h, which agrees perfectly with our observation (70.7% of BnOH consumed after 2.5 h), and up to 100% after 5 h. The same is true for TOF values reported by Das et al. (110 h^{-1} after 5 h; based on the reported values, we calculated a TOF of 140 h^{-1} after 2.5 h),[30] which are identical to those obtained with our experimental setup (139.3 h^{-1} after 2.5 h) despite the lower reaction temperature. However, a marked difference was observed for the selectivity of the oxidation reaction. While Das et al. reported the formation of 93% benzaldehyde and 7% benzoic acid after 5 h, we obtained only 38.5% benzaldehyde and 61.5% benzoic acid with complex **1** after 2.5 h. These findings are in line with the observation of a selectivity increase with increasing steric demand of the carboxylate ligands, as was discussed above when comparing complexes **1** and **2**. In summary, the use of bulkier ligands turned out to be beneficial for enhanced aldehyde selectivity while maintaining, or only slightly reducing, the overall catalytic activity.

EPR Studies

To investigate the appearance of radicals during the oxidation reactions, EPR studies were performed with complex **1** in MeCN solution at ambient temperature in the absence/presence of TBHP/BnOH as well as after heating at 60 °C (Figures S18–S20). Figure 2 shows frozen solution (T = 10 K) EPR spectra of complex **1** in MeCN (top) and the same mixture with TBHP and BnOH (bottom).

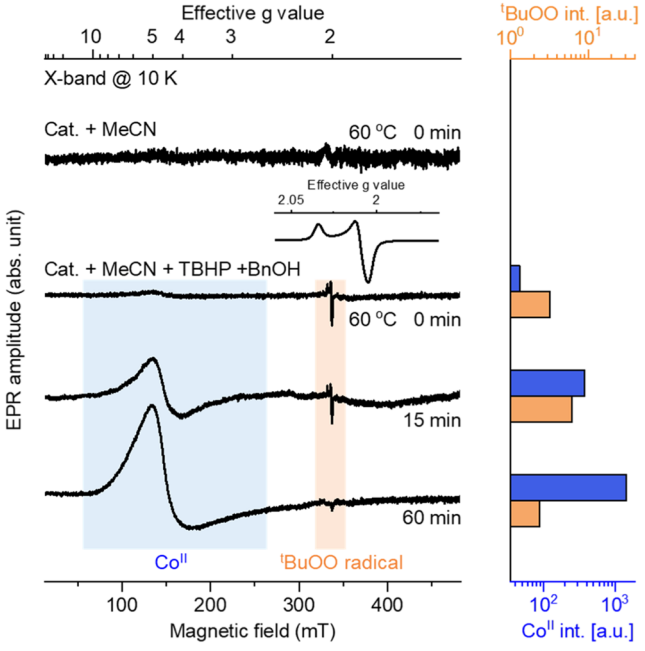
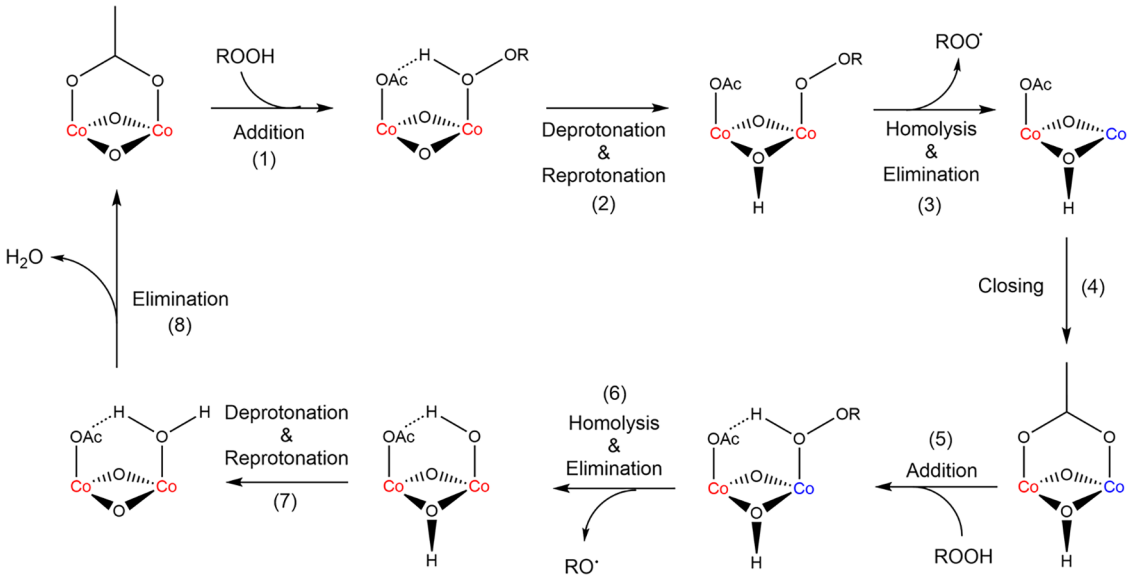


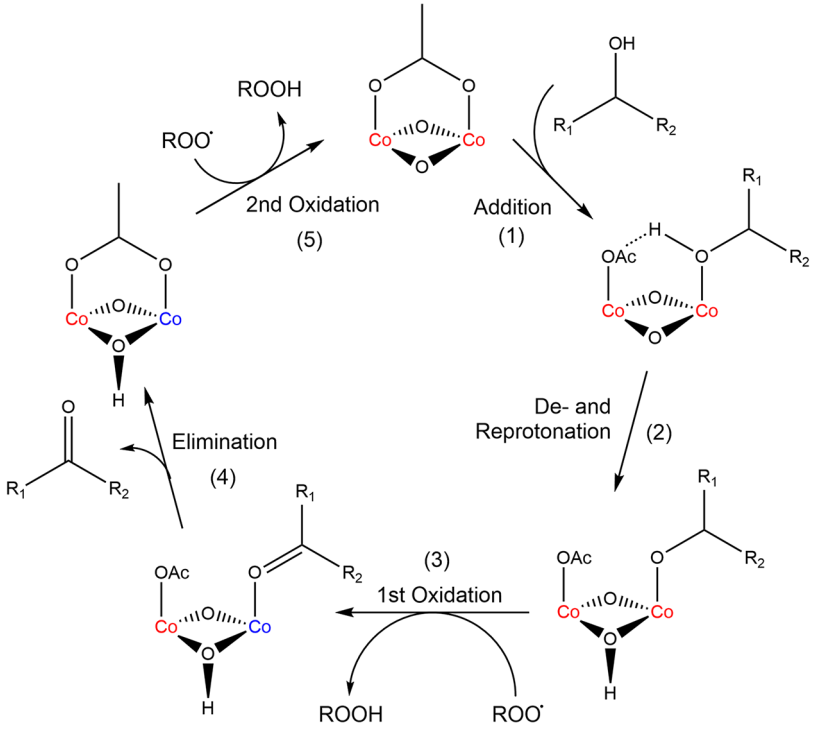
Figure 2. X-band EPR spectra of complex **1** in MeCN at (T = 10 K) after heating at 60 °C. In the presence of TBHP and BnOH, Co^{III} is reduced to Co^{II} (shaded blue) and a *tert*-butyl peroxyl radical (*t*-BuOO$^•$) is formed (orange hatched region and insert). During the reaction the reduction of the Co ions and the formation of *t*-BuOO$^•$ differ in their temporal evolution, as shown in the bar graph of the relative amounts of the two species on the right.

https://doi.org/10.1021/acscatal.5c07998
ACS Catal. 2026, 16, 6355−6367

Scheme 2. Reaction Mechanism for the Hydroperoxide (Oxidant) Activation Pathway (Co^{III}: Red; Co^{II}: Blue; R = *t*-Bu). Only half of the Co_4O_4 heterocubane core are shown.



Scheme 3. Reaction Mechanism for Alcohol Oxidation (Co^{III}: Red; Co^{II}: Blue). Only half of the Co_4O_4 heterocubane core are shown.



Without TBHP and BnOH, no EPR signal was detected, indicating that complex **1** is EPR silent, presumably Co^{III} in the $S = 0$ state. Upon addition of TBHP and BnOH to the reaction mixture, an EPR signal emerged which increased with reaction time. This spectrum is a superposition of a broad signal, characteristic for high spin (HS, $S = 3/2$) Co^{II} (with effective *g*-values of $g^1_{eff} \sim 4.69$, $g^2_{eff} \sim 4.22$, $g^3_{eff} \sim 2.00$ blue hatched area in Figure 2), and a narrow spectrum from *tert*-butyl peroxyl radical (*t*-BuOO•, orange hatched region and insert in Figure 2,[34] $g_1 = 2.034$, $g_2 = 2.010$, $g_3 = 2.004$), respectively.[35] As shown in Figure S21, the emergence of the radical signal occurs only in the presence of TBHP, thereby indicating the formation of *t*-BuOO• radicals. The intensity of the *t*-BuOO• radical signal showed a different time course compared to Co^{II}. While Co^{II} constantly increased during the reaction time of 60 min, the radical amount reached a maximum after 15 min and then decreased. Supporting EPR control experiments with $Co(acac)_2$ and $Co(acac)_3$ showed similar results (Figure S22).

The crucial role of TBHP-derived radicals in the oxidation reactions was further revealed by control experiments in the presence of hydroquinone (0.15 mmol) as a radical scavenger. Hydrochinone is known to act as a radical trap by donating

https://doi.org/10.1021/acscatal.5c07998
ACS Catal. 2026, 16, 6355−6367

hydrogen atoms from its phenolic hydroxyl groups to free radicals. In 2017 Petkovic et al. showed the mechanism of hydroquinone disarms OH and OOH radicals via proton coupled electron transfer.[36] TBHP and complex **1** completely failed to oxidize all three substrates in the presence of one equivalent of hydroquinone (based on TBHP), indicating an active role of radicals in the alcohol oxidation reactions as was confirmed by freeze-quench EPR measurements. Additional spin trap experiments using DMPO (3,4-dihydro-2,3-dimethyl-2*H*-pyrrole 1-oxide) yielded no discernible evidence for the presence of additional radicals derived from BnOH (Figure S21).

Computational Studies

Mechanistic knowledge of the role of tetranuclear $[Co_4^{III}O_4]$ complexes as catalysts in thermal alcohol oxidations is sparse. Amtawong et al.[7] discussed some mechanistic aspects of Co-oxo cubane clusters in oxidation chemistry with a focus on electrocatalysis, particularly water oxidation, rather than on thermal alcohol oxidation. While oxidation states of Co higher than + III (*e.g.*, Co^{IV} or Co^{V}) are relevant under electrochemical conditions,[17,18,37−41] these are assumed to be less accessible in thermal catalysis and thus the mechanisms are expected to be hardly transferable. Heterolytic pathways via Co^{V} appear to be even more unlikely under thermal conditions. In addition, the oxidative role of Co^{III} itself, known from bulk $LaCo_{1-x}Fe_xO_3$ and $Co_{3-x}Fe_xO_4$,[42−44] respectively, should also be considered. Chakrabarty and Das postulated the involvement of alkyl peroxyl intermediates ($ROO^{\bullet}$),[10,22−26,30,45,46] but did not report supporting experimental or computational results. To the best of our knowledge, mechanistic studies on thermal oxidation catalysis at $[Co_4^{III}O_4]$ are limited to cyclohexane oxidation with O_2[47] and to olefin oxidation with *meta*-chloroperoxybenzoic acid,[48] respectively.

We therefore performed a COSMO−DFT(PBE0)/def2-TZVP study on the catalytic activity of $[Co_4^{III}O_4]$ in alcohol oxidation reactions, using the oxidation of BnOH with TBHP and complex **1** as a model reaction. Since the experimental data show no indications for higher Co oxidation states but the involvement of $[Co^{II}]$ and radicals (particularly *t*-$BuOO^{\bullet}$ as indicated from EPR experiments), radical mechanisms and homolytic bond cleavages appeared most probable. Moreover, a mechanism proposed by Frija et al.[49] for the oxidation of secondary alcohols with TBHP at Cu^{II} and Co^{II} catalysts appeared as a promising starting point. Among the different mechanisms investigated, the most favorable pathways are depicted in Schemes 2 and 3. All reaction energies in the following refer to electronic energies corrected by zero-point energy (ZPE) contributions.

First Cycle−Oxidant Activation via a Haber-Weiss Mechanism

Focusing on BnOH/TBHP/**1**, two interrelated catalytic cycles were identified, which explain the catalytic activity of the Co^{III}-oxo cubanes. In the first cycle (Scheme 2), the catalytic oxidation reaction is initiated via a Haber-Weiss activation of TBHP at catalyst **1**, accounting for the transient changes in the Co oxidation state and the generation of peroxyl radicals (*t*-$BuOO^{\bullet}$).

The following steps are involved in hydroperoxide activation:

(1) Addition of TBHP to catalyst **1** accompanied by a change (from μ_2 to μ_1) of the coordination mode of the acetate (AcO^-, Ac = $COCH_3$) ligand
(2) Deprotonation of the coordinated TBHP and protonation of one μ_3-O atom of the $[Co_4O_4]$ cage, yielding a μ_3-bridging hydroxyl (OH) unit
(3) Homolysis of the Co−OO*t*-Bu bond with reduction of $[Co^{III}]$ into $[Co^{II}]$ and subsequent elimination of a *t*-$BuOO^{\bullet}$ radical
(4) (Optional) change of the coordination mode (from μ_1 back to μ_2) of the AcO^- ligand
(5) Binding of a second TBHP molecule at the vacant coordination site
(6) Homolysis of the O−O bond of TBHP under reoxidation of $[Co^{II}]$ to $[Co^{III}]$ and elimination of a *t*-$BuO^{\bullet}$ radical
(7) Deprotonation of the μ_3-bridging hydroxyl (OH) ligand and protonation of the terminal μ_1−OH ligand
(8) Elimination of H_2O or substitution by TBHP

This catalytic cycle can be summarized as two half reactions

$$[Co^{III}(\mu_3\text{-O})] + ROOH \rightarrow [Co^{II}(\mu_3\text{-OH})] + ROO^{\bullet} \quad (1)$$

and

$$[Co^{II}(\mu_3\text{-OH})] + ROOH \rightarrow [Co^{III}(\mu_3\text{-O})] + RO^{\bullet} + H_2O \quad (2)$$

or by the net reaction

$$2ROOH \rightarrow RO^{\bullet} + ROO^{\bullet} + H_2O \quad (3)$$

with a calculated reaction energy for R = *t*-Bu of −2.0 kJ/mol, *i.e.*, slightly exothermic. Due to their higher reactivity, the alkoxyl radicals ($RO^{\bullet}$) are assumed to be short-lived intermediates that quickly react further, particularly by abstracting an H atom from TBHP (−93.9 kJ/mol)

$$RO^{\bullet} + ROOH \rightarrow ROH + ROO^{\bullet} \quad (4)$$

The sum of (eqs 3 and 4) gives a net reaction for the activation of TBHP as

$$3ROOH \rightarrow ROH + 2ROO^{\bullet} + H_2O \quad (5)$$

with a total reaction energy −96.0 kJ/mol. The catalyzed TBHP activation is favored compared to the noncatalyzed activation by bypassing the highly endothermic formation of free $HO^{\bullet}$ radicals

$$ROOH \rightarrow RO^{\bullet} + {}^{\bullet}OH \quad (6)$$

with 153.2 kJ/mol. A comparison of the reaction energies for the individual steps (Table 2) reveals that this cycle is controlled by the energetic cost of ca. 80 kJ/mol starting from $[Co^{III}]$ to reach the $[Co^{II}(\mu_3{-}OH)(ROOH)]$ species (steps 1−5). Its homolytic dissociation (−44.6 kJ/mol) under reoxidation of $[Co^{II}]$ into $[Co^{III}]$ and the generation of $RO^{\bullet}$ alkoxyl radicals as well as the subsequent formation (and elimination) of H_2O (−34.9 kJ/mol) is the driving force of the reaction.

Alternative pathways have also been investigated (Table S1), including (i) a competing homolysis of the O−O bond in $[Co^{III}(ROOH)]$ and consecutive reactions (steps 2a), (ii) the role of different protonation sites (steps 2b), and (iii) the effect of acetate closing ($\mu_1 \rightarrow \mu_2$) in the substitution/elimination reactions (steps 4). Higher oxidation states do not seem to be

https://doi.org/10.1021/acscatal.5c07998
ACS Catal. 2026, 16, 6355−6367

Table 2. Reaction Energies (in kJ/mol) for the Different Steps of the Oxidant (ROOH) Activation via a Haber-Weiss Mechanism Shown in Scheme 2

step	description	TBHP (R = *t*-Bu)	H_2O_2 (R = H)
1	ROOH addition	−3.6	−21.9
2	reprotonation	28.7	15.7
3	homolysis releasing ROO$^\bullet$	88.5	132.2
3a	homolysis releasing RO$^\bullet$	634.3	699.8
3b	heterolysis releasing ROO$^-$	176.7	n. a.
4	closing (optional)	−38.9	−38.9
5	ROOH Addition	2.8	−24.5
6	homolysis releasing RO$^\bullet$	−44.6	17.0
7	reprotonation	−42.4	−42.4
8	elimination of H_2O and closing	7.5	7.5
sum	2 ROOH → RO$^\bullet$ + ROO$^\bullet$ + H_2O	−2.0	44.8

involved as demonstrated for the [Co^{III}]/[Co^{IV}] redox couple (Table S1) due to significantly higher energies, *i.e.*, the initial oxidation of the catalyst (*e.g.*, via electron transfer to ROO$^\bullet$ peroxyl radical) would require 175.3 kJ/mol. Besides, heterolytic pathways generally involve higher energies due to charge separation (as seen for step 3b in Tables 2 and S1).

Second Cycle—Alcohol Oxidation via a Radical Mechanism

In a second catalytic cycle (Scheme 3), BnOH is oxidized at catalyst **1** in a stepwise process.

The following steps are involved:

(1) Addition of $PhCH_2OH$ accompanied by a change (from μ_2 to μ_1) of the coordination mode of one acetate ligand
(2) Deprotonation of coordinated $PhCH_2OH$ and protonation of one μ_3-O atom of the [Co_4O_4] cage, yielding a μ_3-bridging hydroxyl (OH) unit
(3) H abstraction at the C_α atom of the $PhCH_2O$ by a RO$^\bullet$ or ROO$^\bullet$ radical with reduction of [Co^{III}] to [Co^{II}]
(4) Elimination of benzyl aldehyde (PhCHO), leaving behind [Co^{II}], and change of the coordination mode (from μ_1 to μ_2) of the acetate ligand
(5) Reoxidation of [Co^{II}] by RO$^\bullet$ or ROO$^\bullet$ and subsequent deprotonation, restoring the catalyst.

The net reaction of this cycle is

$$R^1R^2CHOH + 2R(O)O^\bullet \rightarrow R^1R^2CO + 2R(O)OH \quad (7)$$

with a reaction energy of −178.5 kJ/mol in the case of BnOH (R^1 = Ph, R^2 = H) and *t*-BuOO$^\bullet$ radicals, the reaction-driving species found by EPR. Together with the activation reaction (eq 5), the overall reaction of TBHP with BnOH is

$$R^1R^2CHOH + ROOH \rightarrow R^1R^2CO + ROH + H_2O \quad (8)$$

with a reaction energy of −180.5 kJ/mol. While the cycle for the oxidant activation is assumed to yield effectively only ROO$^\bullet$ peroxyl radicals, the cycle for the alcohol oxidation could in principle consume any radical species (*i.e.*, HO$^\bullet$, RO$^\bullet$, and ROO$^\bullet$). Apart from an expected reaction energy trend, owing to the varying stability and reactivity of these radicals (Table 3), no relevant differences regarding the oxidation mechanism are observed. In particular, the important C_α−H abstraction and catalyst reoxidation steps are always highly exothermic, acting as the driving force for these oxidations. Moreover, a comparison of the reaction energies for the different steps (Table 3) suggests that the first two steps, *i.e.*, the alcohol addition and its deprotonation, which are both endothermic, control this oxidative cycle.

A comparison with the [Co^{III}]/[Co^{IV}] redox couple (Table S2) revealed that no stable tautomer is formed after deprotonation of the alcohol and reprotonation of a cage oxygen (step 2). Instead, an exothermic rearrangement (−78.4 kJ/mol) was observed (step 2a) which involved an H transfer in the alcoholate from C_α to the cage oxygen atom, yielding [$Co^{IV}(\mu_3$−OH)(PhCHOH)]. The latter species shows a strongly exothermic first H abstraction from the OH group (step 3), but a much more endothermic and, thus, less favorable second H abstraction from [$Co^{III}(\mu_3$−OH)] (step 6) due the energetically more demanding reoxidation of [Co^{III}] into [Co^{IV}]. Particularly, the *t*-BuOO$^\bullet$ radicals are no longer sufficient to give an exothermic reaction. Thus, as for oxidant activation, higher redox couples are not considered relevant for alcohol oxidation.

Comparison of the Oxidants

A comparison between the oxidants TBHP (R = *t*-Bu) and H_2O_2 (R = H) reveals clear energetic differences (Table 3). The formation of the [$Co^{II}(\mu_3$−OH)] species has similar energetic costs (roughly 60 kJ/mol), while the first homolysis for H_2O_2 is less exothermic (132.2 kJ/mol) and the second

Table 3. Reaction Energies (in kJ/mol) for the Different Steps of the Alcohol (R^1R^2CHOH) Oxidation via the Radical Mechanism Shown in Scheme 3

step	description	*i*-PrOH (R^1= Me, R^2 = Me)	BnOH (R^1 = H, R^2 = Ph)	CnOH (R^1 = H, R^2 = PhCHCH)
1	ROH addition	2.5	−7.8	−8.7
2	reprotonation	67.0	44.1	67.0
3a	H abstraction at C_α by HO	−324.3	−288.8	−232.8
3b	H abstraction at C_α by *t*-BuO$^\bullet$	−263.0	−227.6	−171.5
3c	H abstraction at C_α by *t*-BuOO$^\bullet$	−169.1	−133.6	−77.6
4	aldehyde elimination	−15.2	−6.4	−62.4
5	closing (optional)	−38.9	−38.9	−38.9
5a	reoxidation with HO$^\bullet$	−229.9	−233.8	−229.9
5b	reoxidation with *t*-BuO$^\bullet$	−168.6	−172.5	−168.6
5c	reoxidation with *t*-BuOO$^\bullet$	−74.7	−78.6	−74.7
sum	R^1R^2CHOH + 2 RO$^\bullet$ → R^1R^2CHO + 2 ROH			
	oxidation by HO$^\bullet$	−499.7	−488.8	−486.9
	oxidation by *t*-BuO$^\bullet$	−377.3	−366.4	−364.4
	oxidation by *t*-BuOO$^\bullet$	−189.4	−178.5	−176.5

https://doi.org/10.1021/acscatal.5c07998
ACS Catal. 2026, 16, 6355−6367

homolysis is even endothermic (17.0 kJ/mol). This gives a net decomposition of H_2O_2 via the Haber-Weiss mechanism according to

$$2H_2O_2 \rightarrow HO^{\bullet} + HOO^{\bullet} + H_2O \quad (9)$$

with a reaction energy of 44.8 kJ/mol, which is more endothermic than for TBHP. Similarly, the thermal dissociation

$$H_2O_2 \rightarrow 2HO^{\bullet} \quad (10)$$

is also significantly more endothermic (187.5 kJ/mol).

While the net reaction energy (eq 11) suggests that the alcohol oxidation is most efficient with H_2O_2 (*e.g.*, −301.3 kJ/mol for BnOH), this is experimentally not observed due to the kinetic limitations. Although the activation of H_2O_2 via formation of hydroxyl ($HO^{\bullet}$) and hydroperoxyl ($HOO^{\bullet}$) radicals requires more energy associated with higher barriers compared to TBHP, $HO^{\bullet}$ and $HOO^{\bullet}$ can rapidly react under formation of water and oxygen[50]

$$HO^{\bullet} + HOO^{\bullet} \rightarrow H_2O + O_2 \quad (11)$$

The analogue of (eq 11) is not possible for TBHP because the abstraction of a *tert*-butyl group instead of an H atom would be required.

Comparison of the Alcohols

Table 3 compares the energetics of the oxidation mechanism (Scheme 3) with TBHP (and catalyst **1**) of BnOH (*i.e.*, R^1R^2CHOH with R^1 = H, R^2 = Ph) with that for *i*-PrOH (R^1 = R^2 = Me) and CnOH (R^1 = PhCHCH, R^2 = H). The energies for the alcohol addition reactions are similar, whereas the energies for the deprotonation are lower for BnOH and slightly higher for *i*-PrOH and CnOH, reflecting that BnOH is the most acidic among these three alcohols. Overall, *i*-PrOH has the highest energetic cost (ca. 70 kJ/mol) prior to the C_α−H abstraction, while BnOH has the lowest energetic cost (ca. 35 kJ/mol). For CnOH, the activation cost is comparable to that of *i*-PrOH (ca. 60 kJ/mol), but the product elimination is exothermic (−23.5 kJ/mol).

Comparison with Catalyst 2

For the oxidation reactions of *i*-PrOH with H_2O_2 and of BnOH with TBHP, the influence of the catalyst **1** and **2** on the energies for the different steps in the mechanisms was compared. The activation of both oxidants requires slightly higher (more endothermic) reaction energies (Table S3) for the rate-determining steps with catalyst **2**. For the alcohol oxidations (Table S4), a similar trend to more endothermic values (ca. 5−10 kJ/mol higher) is observed, suggesting higher reaction barriers. This is in line with the experimental observations that the conversion rates for the alcohol oxidation reactions are lower but the reactions are more selective with complex **2** compared to **1** (Table 1). This effect is caused by the slightly larger alkyl groups in the carboxylate ligands of **2**, as indicated by the more exothermic product elimination and the coordinative change of the carboxylate ligand (from μ_1 to μ_2, steps 4 and 5 in Table S4).

Comparison with Known Reaction Mechanisms

To the best of our knowledge, only two reaction mechanisms for thermal oxidations at $[Co_4O_4]$ supported by experimental evidence have been reported in the literature. Lee et al.[48] studied olefin oxidation with *meta*-chloroperoxybenzoic acid (mCPBA) at $[Co_4^{II}(OH)_4]$, which is assumed to be initially oxidized into $[Co_4^{III}O_4]$. They reported two distinct reaction pathways: Decomposition of a $[Co^{III}(O_2C(O)R)]$ intermediate via heterolytic bond cleavage involving a $[Co^{V}]$ species results in epoxide formation as the main product, whereas homolytic bond cleavage involving $[Co^{IV}]$ gives the allylic alcohol as a minor product. Gutiérrez-Tarriño et al.[47] investigated cyclohexane oxidation with O_2, proceeding via a radical chain mechanism with cyclohexyl hydroperoxide (CPPH) as a key intermediate and a dual role of the catalyst that assists with O_2 activation and CPPH decomposition.

The alcohol oxidation mechanism described in Scheme 3 was motivated by a mechanism proposed by Frija et al.[49,51] for the oxidation of secondary alcohols with TBHP at mononuclear Cu^{II} and Co^{II} complexes. For the first time, the involvement of alkyl peroxyl intermediates,[52,53] $[Co^{III}(\mu_3\text{−}OH)(OOR)]$, during the oxidant activation, as postulated by Das et al.,[30] could be experimentally proven in this work. For the alcohol oxidation studied here, we observe no involvement of higher oxidation states (*e.g.*, $[Co^{IV}]$ or $[Co^{V}]$), but a dominant preference of homolytic over heterolytic reactions in the alcohol oxidation, in difference to the mechanism proposed by Lee et al. for olefin oxidation. These differences are probably due to the different nature of the oxidants, *i.e.*, TBHP that readily decomposes into radicals and mCPBA, which undergo ionic (heterolytic) reactions. Alternatively, the absence of the alcohol may matter: For example, Morimoto et al.[54] observed the oxidation of secondary alcohols into ketones catalyzed by Co^{III} acetate in the presence of peracetic acid.

The mechanism for the oxidant activation in Scheme 2 has similarities to those for cyclohexane oxidation at $[Co_4O_4]$ reported by Gutiérrez-Tarriño et al.[47] and at $LaCo_{1-x}Fe_xO$ perovskites by Hareendran et al.[42] Despite of different reactants (cyclohexane instead of alcohols), the role of the catalyst in the decomposition of the CPPH intermediate in the latter reactions can be viewed analogous to the activation of TBHP in the current study. Both mechanisms represent a Haber-Weiss-type decomposition of a hydroperoxide that has also been observed by, *e.g.*, Rothenberg et al.[55] The central role of (alkyl) peroxyl radicals has also been described by Denisov and Denisova[56] for the oxidation of alcohols. This suggests that the role of the catalyst in O_2 activation for alkane oxidation as observed by Gutiérrez-Tarriño et al.,[47] should be transferable to alcohol oxidations.

CONCLUSIONS

TBHP is a powerful oxidant for the oxidation of *i*-PrOH, BnOH, and CnOH catalyzed by two tetranuclear Co^{III}-oxo heterocubanes $[Co_4O_4(O_2CR)_4(py)_4]$ (R = Me **1**, Et **2**, py = pyridine) in MeCN as was proven by applying a combination of *in situ* FT-IR and *in situ* ^{1}H NMR spectroscopy. The active role of *t*-$BuOO^{\bullet}$ as the central radical intermediate and the unexpected conversion of Co^{III} into Co^{II} during catalytic reactions were confirmed by freeze-quench and spin-trapping EPR experiments. The experimental results in combination with density functional theory (DFT) calculations finally allowed us to elucidate the catalytic reactions and gain a mechanistic understanding. Two interrelated catalytic cycles were identified, one for the oxidant activation and one for the alcohol oxidation. Key steps of the oxidant activation are (i) the oxidation of ROOH and reduction of Co^{III} into Co^{II} under formation of peroxyl $ROO^{\bullet}$ radicals during the homolysis of a Co−O bond and (ii) the reduction of hydroxyl $HO^{\bullet}$ radicals

https://doi.org/10.1021/acscatal.5c07998
ACS Catal. 2026, 16, 6355−6367

and reoxidation of Co^{II} into Co^{III} under formation of alkoxyl $RO^{\bullet}$ radicals during the homolysis of an O−O bond. Key steps of the alcohol oxidation are (i) an H abstraction at the C_{α} atom by a $ROO^{\bullet}$ radical, (ii) elimination of the aldehyde or ketone, and (iii) reoxidation of the catalyst by another $ROO^{\bullet}$ radical.

Overall, this study provides for the first time a clear mechanistic picture of the role of molecular Co^{III}-oxo cubanes as catalysts in alcohol oxidations, as confirmed by kinetic studies and spectroscopic identification of intermediates together with *ab initio* calculations. An unexpected behavior of the Co^{II}/Co^{III} redox pair and the oxidant TBHP has been revealed, which shares features with the cyclohexane/O_2 oxidation catalyzed by $LaCo_{1-x}Fe_xO$ perovskites.[42] These findings together with the observation that $[Co^{III}]$ is the active species in alcohol oxidation for both $[Co_4O_4]$ and various Co-containing perovskites and spinels (*e.g.*, $CoFe_2O_4$, $LaCo_{1-x}Fe_xO$, Co_3O_4) emphasize the strong link between these molecular model catalysts and solid mixed metal oxide materials.

EXPERIMENTAL SECTION

Materials and Reagents

All reagents were commercially available and used without further purification. The synthesis of complexes **1** and **2** is described in previous work.[13]

In Situ FT-IR Experiments

***In Situ* FT-IR Experiments with TBHP.** *In situ* IR studies were done in MeCN under argon at 82 °C (boiling point of MeCN). The reaction progress was monitored over a period of 6 h using a ReactIR 702L spectrometer (Mettler Toledo) by collecting spectra every 30 s. The initial spectra were subtracted (t = 0 s) from these spectra to improve visibility of the spectral changes.

Reactants were sequentially added at room temperature to a two-necked Ar-filled round-bottom flask under constant stirring (500 rpm) in the following order: 2.0 mL of MeCN, catalyst (**1**, **2**) dissolved in 1.0 mL of MeCN (0.1 mol % based on the alcohol), alcohol (0.75 mol/L based on reaction volume; cinnamyl alcohol was dissolved in 1 mL MeCN), 1.02 mL of TBHP (70% in H_2O), and finally MeCN to reach a total reaction volume of 10 mL. The solution was then heated to 82 °C. The masses and volumes of all components used in the reactions are summarized in Table 4.

Table 4. Summary of the Masses and Volumes Used in the *In Situ* FT-IR Experiments with TBHP (1.02 mL, 70% in H_2O) as an Oxidizing Agent

complex [mg]	alcohol [mL]/[mg]	MeCN [mL]
1 6.39 mg	2-propanol, 0.58 mL	8.40 mL
1 6.39 mg	benzyl alcohol, 0.78 mL	8.20 mL
1 6.39 mg	cinnamyl alcohol, 1.0 g	8.89 mL
2 6.95 mg	2-propanol, 0.58 mL	8.40 mL
2 6.95 mg	benzyl alcohol, 0.78 mL	8.20 mL
2 6.95 mg	cinnamyl alcohol, 1.0 g	8.89 mL

***In Situ* FT-IR Control Experiments with TBHP.** The oxidation reactions with TBHP were repeated using analogous amounts of reagents in the presence of 17 mg of hydroquinone. No alcohol conversion was observed in any of these reactions. In addition, modifications of the BnOH oxidation reaction with TBHP were performed to evaluate the role of the catalyst, alcohol, and TBHP in more detail. After 1 h of reaction time (see above), either (a) 6.39 mg of catalyst **1** dissolved in 1.0 mL of MeCN or (b) 0.78 mL of BnOH or (c) 1.02 mL of TBHP (70% in H_2O) were added and the reaction progress monitored by *in situ* IR spectroscopy.

***In Situ* FT-IR Experiments with O_2.** *In situ* IR studies were performed under an Ar atmosphere in a Parr 4560 Autoclave reactor (450 mL total volume) equipped with a Parr 4848 Reactor Controller unit under constant stirring (500 rpm) at 150 °C. Reaction progress was monitored over a period of 6 h using a ReactIR 702L spectrometer (Mettler Toledo), and spectra were collected every 30 s.

The reaction vessel was purged with Argon and the reagents were sequentially added at room temperature under constant stirring (500 rpm) in the following order: 150 mL of MeCN, 200 mg of the catalyst (**1**) dissolved in 30 mL of MeCN (0.1 mol % based on substrate), the alcohol (1 mol/L based on reaction volume; 20 mL of *i*-PrOH, 20 mL of BnOH, 25.81 g CnOH dissolved in 20 mL of MeCN), and finally MeCN to reach a total reaction volume of 200 mL. The reactor was then closed, the O_2 pressure was set to 10 bar and the mixture was heated to 150 °C. The masses and volumes of all components used in the reactions are summarized in Table 5.

Table 5. Summary of the Masses and Volumes Used in the *In Situ* FT-IR Experiments with 10 bar O_2 as an Oxidizing Agent

complex [mg]	alcohol [mL]/[mg]	MeCN [mL]
1 200 mg	2-propanol, 20 mL	180 mL
1 200 mg	benzyl alcohol, 20 mL	180 mL
1 200 mg	cinnamyl alcohol, 20 g	200 mL

The benzyl alcohol oxidation was repeated once using the same procedure as stated above but with the use of 180 mL of dimethylformamide instead of MeCN to increase the visibility of the conversion (Figure S4).

***In Situ* FT-IR Experiments with H_2O_2.** *In situ* IR studies were done in MeCN under an Ar atmosphere at 82 °C (bp of MeCN). The reaction progress was monitored over a period of 6 h using a ReactIR 702L spectrometer (Mettler Toledo) by collecting spectra every 30 s. The initial spectra were subtracted (t = 0 s) from these spectra to visualize the spectral changes.

Reactants were sequentially added at room temperature to a two-necked Ar-filled round-bottom flask under constant stirring (500 rpm) in the following order: 2.0 mL of MeCN, catalyst (**1**) dissolved in 1.0 mL of MeCN (0.1 mol % based on the alcohol), alcohol (0.75 mol/L based on reaction volume; cinnamyl alcohol was dissolved in 1 mL of MeCN), 0.77 mL of H_2O_2 (30% in H_2O), and finally MeCN to reach a total reaction volume of 10 mL. The solution was then heated to 82 °C. The masses and volumes of all components used in the reactions are summarized in Table 6.

Table 6. Summary of the Masses and Volumes Used in the *In Situ* FT-IR Experiments with 0.77 mL H_2O_2 as an Oxidizing Agent

complex [mg]	alcohol [mL]/[mg]	MeCN [mL]
1 6.39 mg	2-propanol, 0.58 mL	8.40 mL
1 6.39 mg	benzyl alcohol, 0.78 mL	8.20 mL
1 6.39 mg	cinnamyl alcohol, 1.0 g	8.89 mL

All attempted oxidation reactions with H_2O_2 were unsuccessful, even with an increased catalyst concentration (up to 1 mol %/63.9 mg) and a doubled amount of H_2O_2 (1.55 mL).

In Situ ^{1}H NMR Experiments with TBHP

In situ ^{1}H NMR experiments were performed in a *J*-Young NMR tube at 65 °C. The reaction progress was monitored over a period of 6.5 h by acquiring spectra every 5 min using a JNM-ECZL 400 MHz spectrometer (JEOL). The total reaction volume was 0.6 mL, and the amounts of alcohol and MeCN are summarized in Table 7. All reactions were performed with 62 μL of TBHP (70% in H_2O).

To compare the activity and selectivity of the TBHP oxidation reaction of BnOH with those of Das et al.,[30] we repeated the reaction

https://doi.org/10.1021/acscatal.5c07998
ACS Catal. 2026, 16, 6355−6367

Table 7. Amounts of Reagents (mg, mL) Used in *In Situ* ^{1}H NMR Experiments with TBHP (62 μL TBHP, 70% in H_2O) as an Oxidizing Agent as well as Aldehyde Yield (Y), Selectivity (S), and TOF

complex [mg]	substrate [μL]/[mg]	MeCN [μL]	Y [%]	S [%]	TOF [h^{-1}]
1 0.38 mg	2-propanol, 35 μL	503 μL	46.9	100	63.4
1 0.38 mg	benzyl alcohol, 47 μL	491 μL	47.2	53.3	63.8
1 0.38 mg	cinnamyl alcohol, 60 mg	538 μL	76.3	14.2	103.2
2 0.42 mg	2-propanol, 35 μL	503 μL	35.3	100	47.7
2 0.42 mg	benzyl alcohol, 47 μL	491 μL	31.9	77.4	43.1
2 0.42 mg	cinnamyl alcohol, 60 mg	538 μL	49.9	36.2	67.4

with 0.78 mg of catalyst **1**, 47 μL of BnOH, 186 μL of TBHP and 267 μL of MeCN for 2.5h, resulting in a conversion of 70.7%, aldehyde yield of 38.5% (aldehyde selectivity of 54.5%) and a TOF value of 139.3 h^{-1}, respectively.

GC Measurements

Gas chromatography (GC) analysis of the samples originating from alcohol oxidation was performed by using an Agilent 7820A GC system equipped with a flame ionization detector (FID). For cinnamyl alcohol and benzyl alcohol oxidation, an Agilent DB-XLB capillary column (30 m × 0.18 mm × 0.18 μm) was used, whereas for isopropyl alcohol oxidation, an Rtx-Volatiles capillary column (60 m × 0.32 mm ID × 1.50 μm, Catalog No. 10904) was employed. Product quantification was carried out by using the external standard method. Linear calibration curves (R^2 > 0.999) were established by correlating GC peak areas with molar concentrations (Figure S19).

EPR Measurements

X-band cw EPR spectra were obtained using either an X-band Bruker Elexsys E500 EPR spectrometer equipped with an ER4116DM dual mode resonator and an ESR 900 He cryostat at 10K or an MS-5000 (Magnettech GmbH, Freiberg Instruments) at 100−297 K. The samples are prepared in a manner equal to the NMR experiments (see Table 7, complex **1** and BnOH). The EPR spectra at 10 K were obtained using a microwave frequency of ∼9.58 GHz, microwave power of 10 mW, 1400 mT field sweep centered at 700 mT, a Lock-In modulation amplitude of 0.7 mT, a time constant of 20.48 ms and a sweep time of 286.74 s, and a modulation frequency of 100 kHz. The EPR spectra at 100 K were obtained using a microwave frequency of ∼9.48 GHz, microwave power of 1 mW, 50 mT field sweep centered at 337.5 mT, a Lock-In modulation amplitude of 0.3 mT, a sweep time of 60 s, and a modulation frequency of 100 kHz.

The spin trap experiments using DMPO were carried out at 297 K. After the reaction was performed at 60 °C for a certain reaction time, the reaction solution was mixed with 50 mM of DMPO dissolved in MeCN. The mixture was transferred to an EPR tube (OD 1.6 mm × ID 1.0 mm). The tube was placed into the spectrometer, and the spectra were recorded on a Bruker Magnettech ES5000 benchtop spectrometer using the following parameters: magnetic field: 328−348 mT, modulation amplitude: 0.1 mT, microwave frequency: 9.48 GHz, microwave power: 10 mW, sweep time: 10 s, modulation frequency: 100 kHz.

The simulations of the recorded spectra were carried out using "EasySpin", a MATLAB toolbox with "garlic" and "pepper" functions for liquid and frozen solutions.[57]

Quantum-Chemical Calculations

All DFT calculations were done with the TURBOMOLE program package (version 7.9)[58,59] employing the resolution-of-the-identity (RI) approximation. Structures were optimized in solution using DFT (modules ridft and rdgrad)[60−62] with the PBE0[63−65] functional (grid size: m3) in the def2-TZVP basis set[61,66] using default convergence thresholds for the MOs (SCF energy convergence: 10^{-7}; density matrix convergence: 10^{-6}) and during the structure optimization (energy convergence: 10^{-6}; Cartesian gradient convergence: 10^{-3}). The augmented Roothaan-Hall method was used for the MO optimization.[67] To account for solvation effects, the implicit solvent model COSMO (Conductor-like screening model)[68] was used with settings for acetonitrile (relative dielectric constant ε_r = 37.5), the Gaussian charge model,[69] and default settings for the cavity construction. Harmonic frequencies were calculated at the DFT/PBE0/def2-TZVP level using analytic Hessians (with the aoforce module)[70] and used in the calculation of zero-point vibrational energy (ZPVE) corrections to the electronic energies. Structure optimizations and frequency calculations included contributions from the derivatives of integration weights. All molecular structures together with their DFT energies are available in a data publication on Zenodo.[71]

Unrestricted Kohn−Sham (UKS) calculations were used for all open-shell species. Organic radical species with a single unpaired electron were teated in a doublet (S = 1/2) configuration in UKS. For closed-shell structures involving $[Co_4^{III}O_4]$, we exploited the known closed-shell low-spin (S = 0) configuration of Co^{III} in these complexes.[11,30] Complexes involving other Co oxidation states were assumed to have high-spin configurations described by UKS for Co(II) and low-spin configurations for Co(IV) and Co(V), which is in line with the literature on $[Co_3^{III}Co^{V}O_4]^{2+}$ (S = 1),[18] and an approximation for $[Co_3^{III}Co^{IV}O_4]^{+}$ (S = 1/2).[17] The validity of the high-spin assumption for $[Co^{II}Co_3^{III}O_4]^{-}$ has been proven by EPR spectroscopy in this work. All calculations were carefully checked for spin contamination based on the $\langle S^2 \rangle$ expectation values. Information on the oxidation states of the relevant atoms (particularly Co) were determined based on an analysis of the intrinsic bond orbitals[72] and the UKS spin density.

■ ASSOCIATED CONTENT

Supporting Information

The Supporting Information is available free of charge at https://pubs.acs.org/doi/10.1021/acscatal.5c07998.

Experimental IR, ^{1}H NMR, EPR spectra, GC data, and caculated reaction energies (DFT calculation) (PDF)

■ AUTHOR INFORMATION

Corresponding Authors

Alexander Schnegg − *EPR Research Group, Max Planck Institute for Chemical Energy Conversion, 45470 Mülheim an der Ruhr, Germany;* orcid.org/0000-0002-2362-0638; Email: alexander.schnegg@cec.mpg.de

Christof Hättig − *Lehrstuhl für Theoretische Chemie, Ruhr-Universität Bochum, 44780 Bochum, Germany;* orcid.org/0000-0002-5752-2710; Email: christof.haettig@ruhr-uni-bochum.de

Stephan Schulz − *Institute of Inorganic Chemistry, University of Duisburg-Essen, 45141 Essen, Germany; Center for Nanointegration Duisburg-Essen (CENIDE), University of Duisburg-Essen, 47057 Duisburg, Germany;* orcid.org/0000-0003-2896-4488; Email: stephan.schulz@uni-due.de

Authors

Timo Fockenberg − *Institute of Inorganic Chemistry, University of Duisburg-Essen, 45141 Essen, Germany;* orcid.org/0009-0005-8848-3792

Niklas Sülzner − *Lehrstuhl für Theoretische Chemie, Ruhr-Universität Bochum, 44780 Bochum, Germany;* orcid.org/0000-0002-8734-5807

Takuma Sato − *EPR Research Group, Max Planck Institute for Chemical Energy Conversion, 45470 Mülheim an der Ruhr, Germany*

https://doi.org/10.1021/acscatal.5c07998
ACS Catal. 2026, 16, 6355−6367

Dongsheng Zhang − *Laboratory of Industrial Chemistry, Ruhr University Bochum, 44780 Bochum, Germany*
Akhil Hareendran − *Laboratory of Industrial Chemistry, Ruhr University Bochum, 44780 Bochum, Germany;* orcid.org/0000-0001-8884-7668
Jill M. Reher − *Institute of Inorganic Chemistry, University of Duisburg-Essen, 45141 Essen, Germany*
Joana Tewes − *Institute of Inorganic Chemistry, University of Duisburg-Essen, 45141 Essen, Germany*
Martin Muhler − *Laboratory of Industrial Chemistry, Ruhr University Bochum, 44780 Bochum, Germany;* orcid.org/0000-0001-5343-6922

Complete contact information is available at: https://pubs.acs.org/10.1021/acscatal.5c07998

Author Contributions

#T.F. and N.S. contributed equally to this work. T.F.: Experimental, writing manuscript draft and revision. N.S.: DFT calculations, writing manuscript draft and revision. T.S.: EPR measurement, writing manuscript draft and revision. J.M.R.: Experimental. A.H. and D.Z.: GC measurements, revision of the manuscript. M.M.: Supervision, revision of the manuscript. A.S.: Supervision, revision of the manuscript. C.H.: Supervision, revision of the manuscript. S.S.: Supervision, revision of manuscript, resources, project administration. The manuscript was written through contributions of all authors. All authors have given approval to the final version of the manuscript.

Funding

Financial support by the Deutsche Forschungsgemeinschaft (DFG; German Research Foundation) within the Collaborative Research Center/Transregio CRC/TRR 247 "Heterogeneous Oxidation Catalysis in the Liquid Phase" (Project no. 388390466; Projects C03, A05, B06, A01) and Major Research Instrumentation (Project no. 505551334) is acknowledged.

Notes

The authors declare no competing financial interest.

■ ACKNOWLEDGMENTS

We acknowledge support from the University of Duisburg-Essen (S.S.).

■ ABBREVIATIONS

DMPO, 3,4-dihydro-2,3-dimethyl-2H-pyrrole 1-oxide; MeCN, acetonitrile; DTF, density functional theory; EPR, electron paramagnetic resonance; ATR FT-IR, attenuated total reflection Fourier transform infrared; NMR, nuclear magnetic resonance; OER, oxygen evolution reaction; py, pyridine; TBHP, *t*-BuOH, *tert*-butyl hydroperoxide; TOF, turnover frequency; BnOH, benzyl alcohol; CnOH, cinnamyl alcohol; *i*-PrOH, *iso*-propanol (2-propanol).

■ REFERENCES

(1) Nguyen, K. N.; Nguyen, L. B. H.; Bui, T. K.; Nguyen, K. Q.; Van Pham, V. Review of Water Splitting Electrolysis over Cobalt Oxide Nanomaterials. *ACS Appl. Nano Mater.* **2025**, *8*, 3254−3271.
(2) Liu, R.; Wu, H.; Shi, J.; Xu, X.; Zhao, D.; Ng, Y. H.; Zhang, M.; Liu, S.; Ding, H. Recent Progress on Catalysts for Catalytic Oxidation of Volatile Organic Compounds: A Review. *Catal. Sci. Technol.* **2022**, *12*, 6945−6991.
(3) Najafishirtari, S.; Ortega, K. F.; Douthwaite, M.; Pattisson, S.; Hutchings, G. J.; Bondue, C. J.; Tschulik, K.; Waffel, D.; Peng, B.; Deitermann, M.; Busser, G. W.; Muhler, M.; Behrens, M. A Perspective on Heterogeneous Catalysts for the Selective Oxidation of Alcohols. *Chem. - Eur. J.* **2021**, *27* (68), 16809−16833.
(4) Li, K.; Pei, Y.; Xiao, P.; He, Z.; Carabineiro, S. A. C.; Jiang, H.; Zhu, J. Templated Synthesis of Mesoporous Co_3O_4 Nanostructures for the Liquid-Phase Aerobic Oxidation of Benzyl Alcohol to Benzaldehyde. *ACS Appl. Nano. Mater.* **2022**, *5* (3), 3722−3732.
(5) Cordoba, M.; Miranda, C.; Lederhos, C.; Coloma-Pascual, F.; Ardila, A.; Fuentes, G. A.; Pouilloux, Y.; Ramírez, A. Catalytic Performance of Co_3O_4 on Different Activated Carbon Supports in the Benzyl Alcohol Oxidation. *Catalysts* **2017**, *7* (12), No. 384.
(6) Omranpoor, A. H.; Kenmoe, S. 2-Propanol Activation on the Low Index Co_3O_4 Surfaces: A Comparative Study Using Molecular Dynamics Simulations. *Catalysts* **2024**, *14* (1), No. 25.
(7) Amtawong, J.; Nguyen, A. I.; Tilley, T. D. Mechanistic Aspects of Cobalt−Oxo Cubane Clusters in Oxidation Chemistry. *J. Am. Chem. Soc.* **2022**, *144* (4), 1475−1492.
(8) Cox, N.; Pantazis, D. A.; Lubitz, W. Current Understanding of the Mechanism of Water Oxidation in Photosystem II and Its Relation to XFEL Data. *Annu. Rev. Biochem.* **2020**, *89*, 795−820.
(9) Song, F.; Moré, R.; Schilling, M.; Smolentsev, G.; Azzaroli, N.; Fox, T.; Luber, S.; Patzke, G. R. $\{Co_4O_4\}$ and $\{Co_xNi_{4-x}O_4\}$ Cubane Water Oxidation Catalysts as Surface Cut-Outs of Cobalt Oxides. *J. Am. Chem. Soc.* **2017**, *139* (40), 14198−14208.
(10) Chakrabarty, R.; Bora, S. J.; Das, B. K. Synthesis, Structure, Spectral and Electrochemical Properties, and Catalytic Use of Cobalt(III)-Oxo Cubane Clusters. *Inorg. Chem.* **2007**, *46* (22), 9450−9462.
(11) Beattie, J. K.; Hambley, T. W.; Klepetko, J. A.; Masters, A. F.; Turner, P. The Chemistry of Cobalt Acetate - IV. The Isolation and Crystal Structure of the Symmetric Cubane, Tetrakis[(μ-Acetato)(μ_3-Oxo)(Pyridine)Cobalt(III)] • Chloroform Solvate, $[Co_4(\mu_3\text{-}O)_4(\mu\text{-}CH_3CO_2)_4(C_5H_5N)_4]$ • $5CHCl_3$ and of the Dicationic Partial Cubane, Trimeric, [(μ-Acetato)(Acetato)tris(μ-Hydroxy(μ_3-oxo) Hexakispyridinetricobalt(III)]Hexafluorophos-phate • Water Solvate, $[Co_3(\mu_3\text{-}O)(\mu\text{-}OH)_3(\mu\text{-}(CH_3CO_2)(C_5H_5N)_6[PF_6]_2$ • $2H_2O$. *Polyhedron* **1998**, *17* (8), 1343−1354.
(12) Ishaq, M. W.; Nawaz, R.; Jalil, A.; Hashmi, M. A.; Zheng, T.; Li, L. Ligand Exchange Reaction in $[Co_4O_4]$-Cobalt Cubane: A Versatile Strategy Towards the Preparation of Cobalt Cubane-Based Functional Small Molecules and Polymeric Materials. *J. Mol. Struct.* **2021**, *1235*, No. 130216.
(13) Fockenberg, T.; Sülzner, N.; Amin, H. M. A.; Wölper, C.; Hättig, C.; Schulz, S. Synthesis, Characterization, and Electrochemical Properties of Tri- and Tetranuclear Co^{III}-Oxo Complexes. *Eur. J. Inorg. Chem.* **2025**, *28*, No. e202500170.
(14) Nguyen, A. I.; Wang, J.; Levine, D. S.; Ziegler, M. S.; Tilley, T. D. Synthetic Control and Empirical Prediction of Redox Potentials for Co_4O_4 Cubanes over a 1.4 V Range: Implications for Catalyst Design and Evaluation of High-Valent Intermediates in Water Oxidation. *Chem. Sci.* **2017**, *8* (6), 4274−4284.
(15) Li, S.; Zhang, Z.; Marks, W. R.; Huang, X.; Chen, H.; Stoian, D. C.; Erni, R.; Triana, C. A.; Patzke, G. R. $\{Co_4O_4\}$ Cubanes in a Conducting Polymer Matrix as Bio-Inspired Molecular Oxygen Evolution Catalysts. *Nat. Commun.* **2024**, *15*, No. 8432.
(16) Márquez, I.; Gutiérrez-Tarriño, S.; Portorreal-Bottier, A.; del Río-Rodríguez, J. L.; Hernández-Salvador, S.; Calvente, J. J.; Oña-Burgos, P.; Olloqui-Sariego, J. L. Controlled Formation of CoOOH/Co(III)-MOF Active Phase for Boosting Electrocatalytic Alkaline Water Oxidation. *Catal. Today* **2025**, *445*, No. 115049.
(17) McAlpin, J. G.; Stich, T. A.; Ohlin, C. A.; Surendranath, Y.; Nocera, D. G.; Casey, W. H.; Britt, R. D. Electronic Structure Description of a $[Co(III)_3Co(IV)O_4]$ Cluster: A Model for the Paramagnetic Intermediate in Cobalt-Catalyzed Water Oxidation. *J. Am. Chem. Soc.* **2011**, *133* (39), 15444−15452.
(18) Nguyen, A. I.; Ziegler, M. S.; Oña-Burgos, P.; Sturzbecher-Hohne, M.; Kim, W.; Bellone, D. E.; Tilley, T. D. Mechanistic Investigations of Water Oxidation by a Molecular Cobalt Oxide Analogue: Evidence for a Highly Oxidized Intermediate and Exclusive

Terminal Oxo Participation. *J. Am. Chem. Soc.* **2015**, *137* (40), 12865−12872.
(19) Smith, P. F.; Hunt, L.; Laursen, A. B.; Sagar, V.; Kaushik, S.; Calvinho, K. U. D.; Marotta, G.; Mosconi, E.; De Angelis, F.; Dismukes, G. C. Water Oxidation by the $[Co_4O_4(OAc)_4(Py)_4]^+$ Cubium Is Initiated by OH− Addition. *J. Am. Chem. Soc.* **2015**, *137* (49), 15460−15468.
(20) Wang, L. P.; Van Voorhis, T. Direct-Coupling O_2 Bond Forming a Pathway in Cobalt Oxide Water Oxidation Catalysts. *J. Phys. Chem. Lett.* **2011**, *2* (17), 2200−2204.
(21) Fernando, A.; Aikens, C. M. Reaction Pathways for Water Oxidation to Molecular Oxygen Mediated by Model Cobalt Oxide Dimer and Cubane Catalysts. *J. Phys. Chem. C* **2015**, *119* (20), 11072−11085.
(22) Chakrabarty, R.; Das, B. K. Epoxidation of α-Pinene Catalysed by Tetrameric Cobalt(III) Complexes. *J. Mol. Catal. A: Chem.* **2004**, *223* (1−2), 39−44.
(23) Chakrabarty, R.; Kalita, D.; Das, B. K. Catalytic Oxidation of P-Xylene in Water by Cobalt(III) Cubane Cluster. *Polyhedron* **2007**, *26* (6), 1239−1244.
(24) Sarmah, P.; Chakrabarty, R.; Phukan, P.; Das, B. K. Selective Oxidation of Alcohols Catalysed by a Cubane-like Co(III) Oxo Cluster Immobilised on Porous Organomodified Silica. *J. Mol. Catal. A: Chem.* **2007**, *268* (1−2), 36−44.
(25) Das, B. K.; Chakrabarty, R. Cobalt(III)-Oxo Cubane Clusters as Catalysts for Oxidation of Organic Substrates. *J. Chem. Sci.* **2011**, *123* (2), 163−173.
(26) Sarmah, P.; Das, B. K. Catalysis of TBHP Oxidation of Styrene and Diphenylmethane by a Supported Cobalt(III)-Oxo Cluster. *Indian J. Chem., Sect. A* **2014**, *53* (1), 41−45.
(27) Mojet, B. L.; Ebbesen, S. D.; Lefferts, L. Light at the Interface: The Potential of Attenuated Total Reflection Infrared Spectroscopy for Understanding Heterogeneous Catalysis in Water. *Chem. Soc. Rev.* **2010**, *39* (12), 4643−4655.
(28) Pettersson, M.; Tuominen, S.; Räsänen, M. IR Spectroscopic Study of H_2O_2, HDO_2, and D_2O_2 Isolated in Ar, Kr, and Xe Matrices. *J. Phys. Chem. A* **1997**, *101* (6), 1166−1171.
(29) Waffel, D.; Alkan, B.; Fu, Q.; Chen, Y. T.; Schmidt, S.; Schulz, C.; Wiggers, H.; Muhler, M.; Peng, B. Towards Mechanistic Understanding of Liquid-Phase Cinnamyl Alcohol Oxidation with Tert-Butyl Hydroperoxide over Noble-Metal-Free $LaCo_{1-x}Fe_xO_3$ Perovskites. *ChemPlusChem* **2019**, *84* (8), 1155−1163.
(30) Chakrabarty, R.; Sarmah, P.; Saha, B.; Chakravorty, S.; Das, B. K. Catalytic Properties of Cobalt(III)-Oxo Cubanes in the TBHP Oxidation of Benzylic Alcohols. *Inorg. Chem.* **2009**, *48* (14), 6371−6379.
(31) Hempel, M.; Cameron Lampariello, A.; López, N. E.; Springer, C.; McCaskey, K.; Jayaram, S.; Wnuk-Fink, K. M. J.; Werley, B. K.; Funk, T. W. Selectivity Effects of Hydrogen Acceptors and Catalyst Structures in Alcohol Oxidations Using (Cyclopentadienone)Iron Tricarbonyl Compounds. *J. Org. Chem.* **2025**, *90* (5), 2036−2051.
(32) Gildenast, H.; Garg, F.; Englert, U. Sterically Crowded Tris(2-(Trimethylsilyl)Phenyl)Phosphine − Is It Still a Ligand? *Chem. - Eur. J.* **2022**, *28* (7), No. e202103555.
(33) Martins, N. M. R.; Martins, L. M. D. R. S.; Amorim, C. O.; Amaral, V. S.; Pombeiro, A. J. L. First-Row-Transition Ion Metals(II)-EDTA Functionalized Magnetic Nanoparticles as Catalysts for Solvent-Free Microwave-Induced Oxidation of Alcohols. *Catalysts* **2017**, *7* (11), No. 335.
(34) Lommens, P.; Loncke, F.; Smet, P. F.; Callens, F.; Poelman, D.; Vrielinck, H.; Hens, Z. Dopant Incorporation in Colloidal Quantum Dots: A Case Study on Co^{2+} Doped ZnO. *Chem. Mater.* **2007**, *19* (23), 5576−5583.
(35) Jomová, K.; Kysel, O.; Madden, J. C.; Morris, H.; Enoch, S. J.; Budzak, S.; Young, A. J.; Cronin, M. T. D.; Mazur, M.; Valko, M. Electron Transfer from All-Trans β-Carotene to the t-Butyl Peroxyl Radical at Low Oxygen Pressure (an EPR Spectroscopy and Computational Study). *Chem. Phys. Lett.* **2009**, *478* (4−6), 266−270.
(36) Nakarada, Đ.; Petković, M. Mechanistic insights on how hydroquinone disarms OH and OOH radicals. *Int. J. Quantum Chem.* **2018**, *118*, No. e25496.
(37) Ezhov, R.; Ravari, A. K.; Bury, G.; Smith, P. F.; Pushkar, Y. Do Multinuclear 3d Metal Catalysts Achieve O−O Bond Formation via Radical Coupling or via Water Nucleophilic Attack? WNA Leads the Way in $[Co_4O_4]^{n+}$. *Chem. Catal.* **2021**, *1* (2), 407−422.
(38) Ali, A.; Akram, W.; Liu, H. Y. Reactive Cobalt-Oxo Complexes of Tetrapyrrolic Macrocycles and N-Based Ligand in Oxidative Transformation Reactions. *Molecules* **2019**, *24* (1), No. 78.
(39) Brodsky, C. N.; Hadt, R. G.; Hayes, D.; Reinhart, B. J.; Li, N.; Chen, L. X.; Nocera, D. G. In Situ Characterization of Cofacial Co(IV) Centers in Co_4O_4 Cubane: Modeling the High-Valent Active Site in Oxygen-Evolving Catalysts. *Proc. Natl. Acad. Sci. U.S.A.* **2017**, *114* (15), 3855−3860.
(40) Hadt, R. G.; Hayes, D.; Brodsky, C. N.; Ullman, A. M.; Casa, D. M.; Upton, M. H.; Nocera, D. G.; Chen, L. X. X-Ray Spectroscopic Characterization of Co(IV) and Metal-Metal Interactions in Co_4O_4: Electronic Structure Contributions to the Formation of High-Valent States Relevant to the Oxygen Evolution Reaction. *J. Am. Chem. Soc.* **2016**, *138* (34), 11017−11030.
(41) Hodel, F. H.; Luber, S. What Influences the Water Oxidation Activity of a Bioinspired Molecular $Co_4^{II}O_4$ Cubane? An In-Depth Exploration of Catalytic Pathways. *ACS Catal.* **2016**, *6* (3), 1505−1517.
(42) Hareendran, A.; Sato, T.; Dreyer, M.; Rabe, A.; Salamon, S.; Sülzner, N.; Hagemann, U.; Leiva-Leroy, C.; Cosanne, N.; Ravi, K.; Zhang, D.; Busser, G. W.; Behrens, M.; Hättig, C.; Wende, H.; Schnegg, A.; Muhler, M. Mechanistic and Structural Insights into the Liquid-Phase Oxidation of Cyclohexane over $LaCo_{0.7}Fe_{0.3}O_3$ Perovskite Nanoparticles. *ACS Catal.* **2025**, *15*, 12773−12789.
(43) Falk, T.; Budiyanto, E.; Dreyer, M.; Pflieger, C.; Waffel, D.; Büker, J.; Weidenthaler, C.; Ortega, K. F.; Behrens, M.; Tüysüz, H.; Muhler, M.; Peng, B. Identification of Active Sites in the Catalytic Oxidation of 2-Propanol over $Co_{1+x}Fe_{2-x}O_4$ Spinel Oxides at Solid/Liquid and Solid/Gas Interfaces. *ChemCatChem* **2021**, *13* (12), 2942−2951.
(44) Waffel, D.; Budiyanto, E.; Porske, T.; Büker, J.; Falk, T.; Fu, Q.; Schmidt, S.; Tüysüz, H.; Muhler, M.; Peng, B. Investigation of Synergistic Effects between Co and Fe in $Co_{3-x}Fe_xO_4$ Spinel Catalysts for the Liquid-Phase Oxidation of Aromatic Alcohols and Styrene. *Mol. Catal.* **2020**, *498*, No. 111251.
(45) Das, B. K.; Clark, J. H. A Novel Immobilised Cobalt(III) Oxidation Catalyst. *Chem. Commun.* **2000**, No. 7, 605−606.
(46) Chakrabarty, R.; Das, B. K.; Clark, J. H. Enhanced Selectivity in Green Catalytic Epoxidation Using a Supported Cobalt Complex. *Green Chem.* **2007**, *9* (8), 845−884.
(47) Gutiérrez-Tarriño, S.; Gaona-Miguélez, J.; Oña-Burgos, P. Tailoring the Electron Density of Cobalt Oxide Clusters to Provide Highly Selective Superoxide and Peroxide Species for Aerobic Cyclohexane Oxidation. *Dalton Trans.* **2021**, *50* (42), 15370−15379.
(48) Lee, S. Y.; Kim, N.; Lee, M. M.; Jo, Y. D.; Bae, J. M.; Hyun, M. Y.; Yoon, S.; Kim, C. A. Discrete $\{Co_4(\mu_3\text{-}OH)_4\}^{4+}$ Cluster with an Oxygen-Rich Coordination Environment as a Catalyst for the Epoxidation of Various Olefins. *Dalton Trans.* **2016**, *45* (4), 1727−1736.
(49) Frija, L. M. T.; Alegria, E. C. B. A.; Sutradhar, M.; Cristiano, M. L. S.; Ismael, A.; Kopylovich, M. N.; Pombeiro, A. J. L. Copper(II) and Cobalt(II) Tetrazole-Saccharinate Complexes as Effective Catalysts for Oxidation of Secondary Alcohols. *J. Mol. Catal. A Chem.* **2016**, *425*, 283−290.
(50) Weiss, J. The Free Radical Mechanism in the Reactions of Hydrogen Peroxide. *Adv. Catal.* **1952**, *4*, 343−365.
(51) Frija, L. M. T. A Convenient TBHP/$Cu(NO_3)_2{\cdot}2.5H_2O$-Mediated Oxidation of Secondary and Benzyl Alcohols under Microwave Irradiation. *J. Chem. Sci.* **2025**, *137* (3), No. 60.
(52) Saussine, L.; Brazi, E.; Robine, A.; Mimoun, H.; Fischer, J.; Weiss, R. Cobalt(III) Alkylperoxy Complexes. Synthesis, x-Ray Structure, and Role in the Catalytic Decomposition of Alkyl

https://doi.org/10.1021/acscatal.5c07998
ACS Catal. 2026, 16, 6355−6367

Hydroperoxides and in the Hydroxylation of Hydrocarbons. *J. Am. Chem. Soc.* **1985**, *107* (12), 3534−3540.
(53) Talsi, E. P.; Chinakov, V. D.; Babenko, V. P.; Sidelnikov, V. N.; Zamaraev, K. I. Role of Alkylperoxo Complexes of Cobalt (III) in Catalytic Oxidation of Cyclohexane by Cumene Hydroperoxide in the Presence of Bis (Acetylacetonato) Cobalt (II). *J. Mol. Catal.* **1993**, *81* (2), 215−233.
(54) Morimoto, T.; Hirano, M.; Wachi, M.; Murakami, T. Oxidation of Alcohols to Carbonyl Compounds with Peracetic Acid Catalysed by Cobalt (III) Acetate. *J. Chem. Soc., Perkin Trans. 2* **1984**, No. 12, 1949−1951.
(55) Rothenberg, G.; Feldberg, L.; Wiener, H.; Sasson, Y. Copper-Catalyzed Homolytic and Heterolytic Benzylic and Allylic Oxidation Using Tert-Butyl Hydroperoxide. *J. Chem. Soc., Perkin Trans. 2* **1998**, No. 11, 2429−2434.
(56) Denisov, E. T.; Denisova, T. G. Oxidation of Alcohols Involving Two Types of Peroxyl Radicals. *Pet. Chem.* **2006**, *46* (5), 305−313.
(57) Stoll, S.; Schweiger, A. EasySpin, a comprehensive software package for spectral simulation and analysis in EPR. *J. Magn. Reson.* **2006**, *178*, 42−55.
(58) TURBOMOLE V7.9 2024. *Adevelopment of University of Karlsruhe and Forschungszentrum Karlsruhe GmbH, 1989−2007*; TURBOMOLE GmbH, since 2007 https://www.turbomole.orghttps://www.turbomole.org.
(59) Franzke, Y. J.; Holzer, C.; Andersen, J. H.; Begušić, T.; Bruder, F.; Coriani, S.; Sala, F. D.; Fabiano, E.; Fedotov, D. A.; Fürst, S.; Gillhuber, S.; Grotjahn, R.; Kaupp, M.; Kehry, M.; Krstić, M.; Mack, F.; Majumdar, S.; Nguyen, B. D.; Parker, S. M.; Pauly, F.; Pausch, A.; Perlt, E.; Phun, G. S.; Rajabi, A.; Rappoport, D.; Samal, B.; Schrader, T.; Sharma, M.; Tapavicza, E.; Treß, R. S.; Voora, V.; Wodyński, A.; Yu, J. M.; Zerulla, B.; Furche, F.; Hättig, C.; Sierka, M.; Tew, D. P.; Weigend, F. TURBOMOLE: Today and Tomorrow. *J. Chem. Theory Comput.* **2023**, *19* (20), 6859−6890.
(60) Eichkorn, K.; Weigend, F.; Treutler, O.; Ahlrichs, R. Auxiliary Basis Sets for Main Row Atoms and Transition Metals and Their Use to Approximate Coulomb Potentials. *Theor. Chem. Acc.* **1997**, *97* (1−4), 119−124.
(61) Eichkorn, K.; Treutler, O.; Öhm, H.; Häser, M.; Ahlrichs, R. Auxiliary Basis Sets to Approximate Coulomb Potentials. *Chem. Phys. Lett.* **1995**, *242* (6), 652−660.
(62) Treutler, O.; Ahlrichs, R. Efficient Molecular Numerical Integration Schemes. *J. Chem. Phys.* **1995**, *102* (1), 346−354.
(63) Perdew, J. P.; Wang, Y. Accurate and Simple Analytic Representation of the Electron-Gas Correlation Energy. *Phys. Rev. B* **1992**, *45* (23), No. 13244.
(64) Perdew, J. P.; Burke, K.; Ernzerhof, M. Generalized Gradient Approximation Made Simple. *Phys. Rev. Lett.* **1996**, *77* (18), No. 3865.
(65) Perdew, J. P.; Ernzerhof, M.; Burke, K. Rationale for Mixing Exact Exchange with Density Functional Approximations. *J. Chem. Phys.* **1996**, *105* (22), 9982−9985.
(66) Weigend, F.; Ahlrichs, R. Balanced Basis Sets of Split Valence, Triple Zeta Valence and Quadruple Zeta Valence Quality for H to Rn: Design and Assessment of Accuracy. *Phys. Chem. Chem. Phys.* **2005**, *7* (18), 3297−3305.
(67) Høst, S.; Olsen, J.; Jansík, B.; Thøgersen, L.; Jørgensen, P.; Helgaker, T. The augmented Roothaan−Hall method for optimizing Hartree−Fock and Kohn−Sham density matrices. *J. Chem. Phys.* **2008**, *129*, No. 124106.
(68) Schäfer, A.; Klamt, A.; Sattel, D.; Lohrenz, J. C. W.; Eckert, F. COSMO Implementation in TURBOMOLE: Extension of an Efficient Quantum Chemical Code towards Liquid Systems. *Phys. Chem. Chem. Phys.* **2000**, *2* (10), 2187−2193.
(69) Pausch, A. Consistent Analytical Second Derivatives of the Kohn−Sham DFT Energy in the Framework of the Conductor-Like Screening Model through Gaussian Charge Distributions. *J. Chem. Theory Comput.* **2024**, *20* (8), 3169−3183.
(70) Deglmann, P.; May, K.; Furche, F.; Ahlrichs, R. Nuclear Second Analytical Derivative Calculations Using Auxiliary Basis Set Expansions. *Chem. Phys. Lett.* **2004**, *384* (1−3), 103−107.
(71) Sülzner, N.; Hättig, C. *Comparative Study on the Catalytic Activity of [$Co_4^{III}O_4$] Heterocubanes in Alcohol Oxidation Reactions in Solution*. Zenodo, 2023. DOI: 10.5281/zenodo.17486850.
(72) Knizia, G. Intrinsic Atomic Orbitals: An Unbiased Bridge between Quantum Theory and Chemical Concepts. *J. Chem. Theory Comput.* **2013**, *9* (11), 4834−4843.



https://doi.org/10.1021/acscatal.5c07998
ACS Catal. 2026, 16, 6355−6367